SCIENTIFIC REPORTS

OPEN

Geobiology reveals how human kidney stones dissolve *in vivo*

Mayandi Sivaguru[1,2], Jessica J. Saw[1,3,4], James C. Williams Jr.[5], John C. Lieske[6,7], Amy E. Krambeck[8,9], Michael F. Romero[10], Nicholas Chia[10,11], Andrew L. Schwaderer[12], Reinaldo E. Alcalde[13], William J. Bruce[14], Derek E. Wildman[1,3], Glenn A. Fried[1,2], Charles J. Werth[13], Richard J. Reeder[15], Peter M. Yau[16], Robert A. Sanford[1,17] & Bruce W. Fouke[1,2,17,18,19]

Received: 9 April 2018
Accepted: 29 August 2018
Published online: 13 September 2018

More than 10% of the global human population is now afflicted with kidney stones, which are commonly associated with other significant health problems including diabetes, hypertension and obesity. Nearly 70% of these stones are primarily composed of calcium oxalate, a mineral previously assumed to be effectively insoluble within the kidney. This has limited currently available treatment options to painful passage and/or invasive surgical procedures. We analyze kidney stone thin sections with a combination of optical techniques, which include bright field, polarization, confocal and super-resolution nanometer-scale auto-fluorescence microscopy. Here we demonstrate using interdisciplinary geology and biology (*geobiology*) approaches that calcium oxalate stones undergo multiple events of dissolution as they crystallize and grow within the kidney. These observations open a fundamentally new paradigm for clinical approaches that include *in vivo* stone dissolution and identify high-frequency layering of organic matter and minerals as a template for biomineralization in natural and engineered settings.

Kidney stones have been formally studied by western medicine since 1802[1,2]. In 1868, Beale[3] reported that urine contains suspended crystal sediments of calcium oxalate (CaOx, oxalate of lime) that are "difficult" to dissolve. Research then focused on mineralogy, chemistry and protein incorporation as primary controls on stone growth, with little evaluation of urine chemistry[4–6]. These minerals originally form as tetragonal bipyramid crystals of CaOx dihydrate (COD; *Weddellite*; $CaC_2O_4 \cdot 2H_2O$) that "transform during the partial loss of water" into monoclinic lozenge-shaped crystals of CaOx monohydrate (COM; *Whewellite*; $CaC_2O_4 \cdot H_2O$)[7–9]. A third common but minor mineral phase in CaOx stones is orthorhombic crystalline uric acid (UA; $C_5H_4N_4O_3$)[10]. During the 1960s, stone research transitioned to focus on the role of 24-hour urine solution chemistry and calculated supersaturation as an index of stone formation risk[11]. It is now known that a complex variety of factors other than simple urine chemistry influence stone formation, including protein degradation products, cellular responses, and even

[1]Carl R. Woese Institute for Genomic Biology, University of Illinois at Urbana-Champaign, Urbana, IL, USA. [2]Carl Zeiss Labs@Location Partner, Carl R. Woese Institute for Genomic Biology University of Illinois at Urbana-Champaign, Urbana, IL, USA. [3]Department of Molecular and Integrative Physiology, University of Illinois at Urbana- Champaign, Urbana, IL, USA. [4]Mayo Clinic School of Medicine, Mayo Clinic, Rochester, MN, USA. [5]Department of Anatomy and Cell Biology, Indiana University School of Medicine, Indianapolis, IN, USA. [6]Division of Nephrology and Hypertension, Mayo Clinic, Rochester, MN, USA. [7]Department of Laboratory Medicine and Pathology, Mayo Clinic, Rochester, MN, USA. [8]Department of Urology, Mayo Clinic, Rochester, MN, USA. [9]Department of Urology, Indiana University School of Medicine, Indianapolis, IN, USA. [10]Department of Physiology & Biomedical Engineering, Mayo Clinic, Rochester, MN, USA. [11]Department of Individualized Medicine, Mayo Clinic, Rochester, MN, USA. [12]Department of Pediatric Nephrology, Indiana University School of Medicine, Indianapolis, IN, USA. [13]Civil, Architectural and Environmental Engineering, University of Texas at Austin, Austin, TX, USA. [14]Loyola University Chicago, Stritch School of Medicine, Maywood, IL, USA. [15]Department of Geosciences, Stony Brook University, Stony Brook, NY, 11794, USA. [16]Protein Sciences, Roy J. Carver Biotechnology Center, University of Illinois at Urbana-Champaign, Urbana, IL, USA. [17]Department of Geology, University of Illinois at Urbana-Champaign, Urbana, IL, USA. [18]Department of Microbiology, University of Illinois at Urbana-Champaign, Urbana, IL, USA. [19]Roy J. Carver Biotechnology Center, University of Illinois at Urbana-Champaign, Urbana, IL, USA. Mayandi Sivaguru, Jessica J. Saw and Bruce W. Fouke contributed equally. Correspondence and requests for materials should be addressed to M.S. (email: sivaguru@illinois.edu) or J.J.S. (email: jsaw2@illinois.edu) or B.W.F. (email: fouke@illinois.edu)

the likely presence of a kidney microbiome[12–14]. Moreover, a host of complex human health conditions including dehydration, pregnancy, diet, diabetes, hypertension, obesity, genetics, and climate[12,15] also affects kidney stone susceptibility. Thus, current clinical strategies to employ hydration, diet and/or drugs to "correct" urine chemistry are at best only partially effective in preventing stone growth.

In the present study, more than 50 CaOx kidney stone fragments, collected from six Mayo Clinic patients during standard percutaneous nephrolithotomy (PCNL) procedures, are analyzed. Integrated geology and biology (*geobiology*) techniques are applied within the chronological and spatial framework of crystal growth and stratigraphic layering patterns (*crystalline architecture*) that comprise each stone fragment. Bulk mineralogical analyses with infrared (IR) spectroscopy confirm that all samples are primarily composed of CaOx (see Methods). We analyze ~20 μm-thick stone fragment sections polished on both sides using a wide range of optical microscopy (250 nm-resolution), which include brightfield, phase contrast, polarization, single- and two-photon spectral confocal, and fluorescence lifetime imaging. In addition, we use Airyscan super-resolution microscopy (~140 nm-resolution) to bring the optical resolution beyond the diffraction limit of light[16–18]. To determine mineralogy and chemistry in thin section, we use scanning electron microscopy and energy-dispersive x-ray spectroscopy. Only stone fragments from patient MP2 contain all events of crystalline architecture collectively identified in all six patient specimens. Therefore, we present MP2 as an exemplar of CaOx kidney stone growth.

Our microscopy analyses indicate that extensive and repeated dissolution occurs throughout the growth history of each stone. This evidence stands in stark contrast to the common perception that kidney stones do not dissolve in the human kidney[3,12,15]. These results suggest multiple novel strategies targeting *in vivo* dissolution may be effective in alleviating the adverse health impacts of this increasingly common disease. At the same time, these insights broaden and advance our ability to accurately interpret the physical, chemical and biological processes that control mineral deposition in a variety of other human diseases, as well as many other natural and engineered environments where biomineralization takes place.

Results and Discussion

Historical sequence of events. Distinct stratigraphic layering on the scale of 10's to 100's of nanometers (*nano-layering*) is revealed by auto-fluorescence (AF, emission of a specific fluorescence light without labels in response to a specific excitation wavelength)[16,17] generated by changes in organic matter composition (Supplementary Fig. 1). We interpret the crystalline architecture of COD, COM and UA in kidney stones using the Law of Superposition (i.e., older layers at the bottom and younger layers at the top), proposed in 1667 by Nicholas Steno, a Danish physician and pioneering geobiologist[2,19]. Our observations are synthesized into a historical sequence of events (HSE, Fig. 1, a *paragenetic sequence* in geology)[20].

The earliest stage of kidney stone growth begins with the precipitation of 5–250 μm-diameter perfectly geometrically formed (*euhedral*) COD and COM with internal concentric zonations consistent with free-floating growth in the renal calyx and/or pelvis (i.e., *crystalline sediment* or *crystalluria*)(COD_{FF} and COM_{FF}, HSE 1 in Figs. 1 and 2a)[21,22]. The outermost surfaces of larger COD_{FF} have euhedral extensions reflecting crystal twinning[21], including the adherence of smaller COD_{FF} to other larger COD_{FF} faces[23] in the form of aggregates (HSE 2 in Figs. 1, 2a and Supplementary Fig. 2a). These outermost surfaces then dissolve (HSE 3 in Figs. 1 and 2a), cutting 10's of microns down into internal concentric COD_{FF} layers. Following dissolution, small <5–10 μm-diameter COM_{FF} land on and encrust outer COD_{FF} surfaces (Figs. 1c and 2a). The next generation of COM exhibits a dense nano-layered cortex (COM_C; HSE 4 in Figs. 1, 2a and Supplementary Fig. 2b)[24,25] that encrusts both pristine and dissolved COD_{FF} surfaces. In addition, some COM_{FF} land on and are then encrusted by the same COM_C (HSE 4 in Figs. 1 and 2a). COM_C generally adopts the same crystallographic C-axis orientation as the COD_{FF} and COM_{FF} (Fig. 1c) they encrust (*syntaxial overgrowths*).

The COD_{FF}, COM_{FF} and COM_C crystal complex then extensively and repeatedly dissolves (HSE 5 in Figs. 1, 2a), which is recorded by four types of fabrics that cross-cut the crystalline architecture (Supplementary Fig. 2a–d): (1) Micron-sized and larger crystals of COD_{FF} partially dissolve from their center, creating irregular void spaces lined with remnants of original COD_{FF} (white arrowheads in Figs. 1c, 2a, Supplementary Fig. 2c). (2) Bulk dissolution completely removes the original COM_C-encrusted COD_{FF}, leaving euhedral mold-shaped void spaces (*moldic porosity*, P in Figs. 1, 2 and Supplementary Fig. 2a–d). (3) Continued bulk dissolution cuts into COM_C, creating canyon-like void spaces that cross-cut COM_C nano-layering (Fig. 2b and Supplementary Fig. 2d. (4) Both irregular and euhedral moldic porosity within COD_{FF}, COM_{FF}, and COM_C is then partially to completely filled with replacement COM (COM_R; HSE 6 in Figs. 1, 2a,b and Supplementary Fig. 2b,c,e–g). In addition, Ångstrom-scale dissolution and crystallization (*mimetic replacement*, COM_M) of COM_C takes place, in which the original fine laminations of the cortex are completely to partially preserved (HSE 6 in Figs. 1, 2a and Supplementary Fig. 3).

The final stage of stone growth occurs when three separate stone fragments come into contact, locally dissolve at contact points and interlock to create a larger stone complex (Supplementary Fig. 1b,c and Video 1). At present, we cannot distinguish if the three stone fragments formed entirely by naturally occurring events within the patient's kidney, or whether they broke apart as a result of previous medical intervention. The margins of each fragment are irregular, intertwined and exhibit large-scale 300–400 μm-scale truncation of COM_C nano- layering (Supplementary Fig. 1b,d). These data indicate that dissolution continues as the margins of the stones come into contact. After the fragments merge into a stone complex, COM then grows on some outer stone surfaces as cements (COM_{CE}; lime green layers in Supplementary Fig. 1c, labeled COM_{CE} in Fig. 2c and Supplementary Fig. 4a,b), which exhibit crystal-face specific differences in organic matter concentrations (*sector zoning*) (labeled SZ in Fig. 2c and Supplementary Fig. 4b)[26]. Uric acid cement crystals (UA_{CE}) then grow on outer surfaces of the stone complex (gray layers in Supplementary Fig. 1c, labeled UA_{CE} in Fig. 2c and Supplementary Fig. 4a,b). Other outermost COM_C stone surfaces continue to dissolve and are replaced by COD and COM (COD_R and COM_R, cyan in Supplementary Figs. 1c, 4c–f), which is consistent with previously observed "intimate COD and COM relationships[6]".

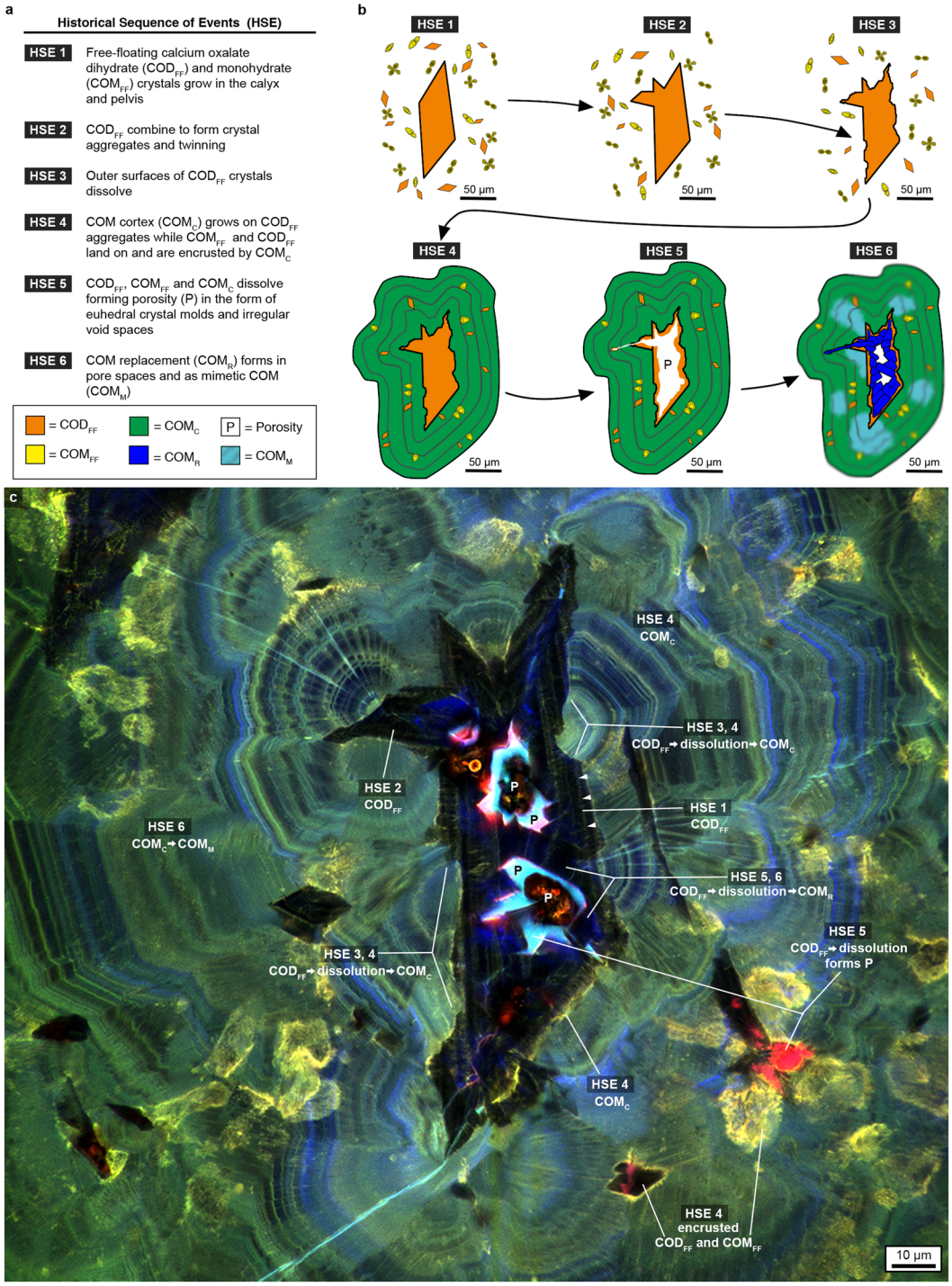

Figure 1. Historical sequence of events (HSE) constructed from super-resolution auto-fluorescence (SRAF) images of the MP2 calcium oxalate (CaOx) kidney stone. (**a**) The HSE. (**b**) Sketch depicting individual HSE events. (**c**) Representative SRAF image composed of merged three pseudo-colored red, green and blue (RGB) channels. Brightness and contrast of the RGB channel intensities are adjusted to highlight the dark crystalline fabrics. Raw images with and without adjustments are presented in Supplementary Fig. 2.

COD_{FF} aggregates, which reach 300 µm in diameter (dark blue S3 in Supplementary Fig. 1c), are consistent with previous observations of COD morphology within kidney stones and likely form under hypercalciuric conditions[27]. Their large size requires that crystals aggregate in urine collected in the renal calyx and pelvis as opposed to filtrate in the nephron collecting ducts, which only reach ~150 µm in diameter[12,15]. These large COD_{FF} aggregates form the nucleus (*nidus*) that COM_C encrusts (Fig. 1c). The symmetry of the COM_C concentric layering indicates free-floating crystallization while completely bathed in urine. Growth while attached to tissue on one side would create discontinuous and asymmetric COM_C layering around the COD_{FF} nidus[12,15]. In addition,

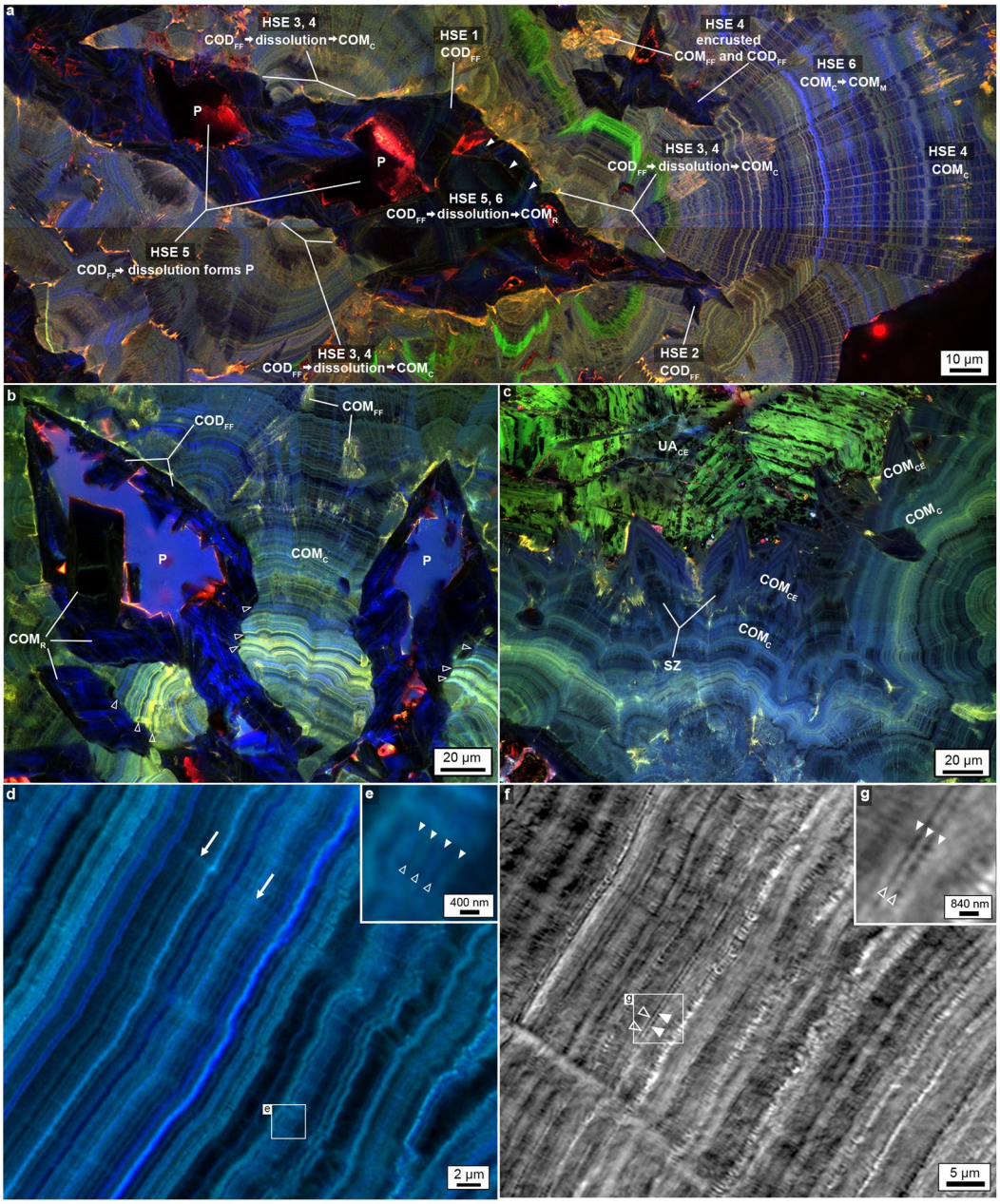

Figure 2. Evidence for *in vivo* dissolution and nano-layering from confocal auto-fluorescence (CAF) and SRAF imaging of the MP2 CaOx kidney stone. Specific areas of the MP2 stone from which these image enlargements are made are shown in Supplementary Fig. 1. (**a**) Tiled CAF image of merged pseudo-colored RGB channels with no image adjustments. (**b**,**c**) SRAF images of merged pseudo-colored RGB channels. The brightness and contrast of each image is individually adjusted to highlight the layered crystalline architecture (raw images with and without adjustments are presented in Supplementary Fig. 22). (**d**) SRAF image of COM_C nano-layering from merged two-channel blue and red (pseudo-colored cyan) channels (Z-stack optical sections of all layers are presented in Supplementary Video 2). The SRAF green channel is identical to the red channel (pseudo-colored cyan) and therefore not included. (**e**) Individual ~140 nm-thick dark and light nano-layers (open and closed arrowheads) with enlargement (**e**). Radiating twinned crystals grow with their c-axis oriented perpendicular to each dark or light nano-layer (arrows). (**f**) Black and white circular polarization phase contrast (CPOLPC) image shows COM_C dark organic matter-rich and light mineral-rich nano-layering with enlargement (**g**). The original color image of the same area is presented in Supplementary Fig. 18. Images (**d**,**e**) are displayed with best-fit intensity profiles. Images (**f**,**g**) are displayed with best-fit intensity profiles after a gamma correction of 0.4.

COM_{FF} are observed to have landed on the growing surfaces of COM_C. These crystals become entombed in, and encrusted by, the concentric COM_C nano-layering (Figs. 1c and 2, Supplementary Fig. 4c,d) and are called protrusions[28] into COM_C.

The HSE (Fig. 1) of this representative stone has broad implications for understanding the growth history of other types of kidney stones, including those that originate in the renal papilla as interstitial deposits of calcium phosphate (*apatite*) called Randall's plaques, or in the ducts of Bellini called Randall's plugs[29–31]. Randall's plaque commonly erupt into the renal calyx and pelvis, or are released through the nephron, and begin to accrete COD_{FF} and eventually COM_C (HSE 4) while bathed in urine[12]. Instead of the initial stages of apatite nidus growth[32], CaOx kidney stones in the present study have a nidus composed of free-floating COD_{FF} and COM_{FF} (HSE 1–3, Fig. 1). The lack of apatite crystal dissolution fabrics within COD_{FF} and COM_C in the MP-series stone fragments implies that these CaOx stone fragments likely did not contain a precursor Randall's plaque or plug nidus.

Kidney stones dissolve *In vivo*. Results from the current study modify the long-held working assumption that COM is strongly insoluble *in vivo*[3,12,15], except perhaps within some individual cell organelles (*phagolysosomes*)[33]. In addition, although the entombment of organic matter has been previously documented[12,15], the clinical importance of these biomass-rich nano-layers remains undetermined[28]. Our results indicate that kidney stones repeatedly dissolve *in vivo* (Figs. 1 and 2, Supplementary Figs. 1–4; summarized as dissolution of COD_{FF} outer surfaces [HSE 3], dissolution of COD_{FF}, COM_{FF} and COM_C via four types of cross-cutting crystal fabrics [HSE 5], and mimetic replacement of COM_C by COM_M [HSE 6]) and highlight the intrinsic relationship between organic-rich and mineral-rich nano-layering.

The repeated dissolution, crystallization and resultant remodeling of crystalline architecture that takes place during CaOx stone growth is analogous to the commonly observed post-depositional physical, chemical and biological alteration observed in natural mineral deposits (*diagenesis*)[24]. The sector zoning in COM_{CE} indicates that these crystals may be more soluble and thus more susceptible to diagenesis than expected with respect to calculated urine supersaturation states[25], as controlled by the differential entrapment of organic matter on specific COM crystal faces[34,35]. The biomolecules present within the human kidney may also play a major role in driving the multiple events of dissolution as recorded in the HSE (Fig. 1). These are normal constituents of urine chemical composition[36], and could plausibly include biomolecules derived from a resident microbial community (*microbiome*)[13]. However, the composition and potential effects of these biomolecules are currently unknown[37].

COM_C nano-layers. We use fast Fourier transform (FFT) frequency analyses to compare the nano-layering within individual COM_C, COD_{FF} and COM_R (Supplementary Fig. 5). Both COM_C and COD_{FF} exhibit highest frequencies and thinnest nano-layers (Supplementary Fig. 5a–d,g–j). The crystalline architecture of COM_C, COD_{FF} and COM_R exhibit different patterns in three distinct optical modalities applied (POLPC, CPOL, SRAF, Supplementary Fig. 11) indicating that multi-modal approaches are required to investigate kidney stone crystalline fabrics (Supplementary Fig. 5). Nano-layering is the most volumetrically dominant component of COM_C (Figs. 1 and 2) and occurs in well-defined organic matter- and mineral-rich couplets[12,15,38]. However, a comprehensive understanding of the mechanisms controlling the abrupt switch between deposition of each organic matter-rich and mineral-rich nano-layer is unknown[9,28,39,40]. Under SRAF imaging, bright AF indicates organic matter-rich layers, while dim AF represents the adjacent mineral-rich couplet layers (Fig. 2d,e and Supplementary Figs. 5 and 12). In contrast, when observed under transmitted-light polarization and phase contrast (CPOLPC), the brighter layers are crystal-rich and the dimmer layers are organic matter-rich (Fig. 2f,g). While SRAF imaging reveals sharp well-defined COM_C layer couplets at a spatial resolution as fine as ~140 nm (Fig. 2e), previous transmission electron microscopy imaging of other kidney stones has detected even finer layering at ~50 nm in thickness[41]. If these ~50 nm-thick layers are present in the six Mayo Clinic patient stones, they would not have been optically resolved with SRAF in the present study, but instead, would optically average into ~140 nm-thick layers within each couplet. As a result, the actual number of COM_C layer couplets and their frequencies in the present study could be a 2–3-fold underestimate. Given these detection limits, the observed COM_C is composed of ~140–250 nm couplets based on the optical resolution of our microscope system.

An initial interpretation of these COM_C couplets (Fig. 2d–g) is that the organic matter-rich nano-layers are films of biomolecules (peptides, proteins, etc.) entombed between mineral-rich nano-layers[28]. Potential reasons for these rapid nano-layer shifts might include frequent changes in human host and kidney physiology, urine biochemistry and perhaps even microbiome ecology and activity. Alternatively, these layers are also comparable to the oscillatory zoning found in many minerals, where it is believed that a kinetic feedback mechanism results in periodic oscillations of crystal growth and impurity occlusion independent of biological activity[42]. Further analysis of the composition and concentration of organic matter entrapped in each cortex nano-layer will be required to establish a mechanistic hypothesis for their deposition. Since the exact amount of time required to form any given kidney stone is difficult to constrain, it is uncertain precisely how long it takes to deposit each nano-layer couplet. However, previously published observational data regarding how long it takes CaOx stones to grow[43,44] implies that several thousands of nano-layers could possibly form within weeks or months. Given these rough estimates, each nano-layer may have formed on a sub-daily basis of hours or in some cases even minutes. If correct, kidney stones could be "read" in the future under clinical conditions as an unprecedented ultrahigh-sensitivity record of *in vivo* human renal function and dynamic biogeochemical reactions.

Biomineralization in natural and engineered environments. The alternating organic matter- and mineral-rich nano-layers comprising COM_C are strikingly similar to those seen in other modern and ancient sedimentary deposits. These include marine stromatolites, ooids and oyster shells and pearls, as well as terrestrial hot-spring travertines and cave speleothems, among many other deposits[45–47]. Previous geobiology studies of these natural deposits have only partially deciphered the relative influence of the physical, chemical and biological factors that are active at the time of layered deposition. COM_C nano-layer couplets represent a previously unknown template for understanding the mechanisms that fundamentally control shifts between biotic and abiotic processes during biomineralization. These mechanisms are directly applicable to understanding

biomineralized deposits common to other natural and engineered environments in fields that range from environmental sustainability and energy production, to medical discovery and space exploration.

BF microscopy with a theoretical optical resolution of approximately 1-μm was used to compare the nano-layer couplets in kidney stones (Supplementary Fig. 6a–c,j) with travertine formed within ancient Roman aqueducts[45,47] (Supplementary Fig. 6d–f,k) and cave limestone deposits (*speleothems*, Supplementary Fig. 6g–i,l)[45,46]. Out of necessity, these analyses are completed at a micrometer-scale resolution instead of the nanometer-scale since the cave and aqueduct systems have orders-of-magnitude higher crystal growth rates than those in the kidney (Supplementary Fig. 13). These higher rates of crystal growth dramatically increase the thickness of each layer, which makes only one or two layers fill an entire frame at super-resolution, making them incompatible for frequency analysis (Supplementary Fig. 13a–d). Requirement of lower magnification imaging indicates that CaOx kidney stone layers are 10-times higher frequency (~1.6 μm/layer) than those in the cave deposits (~16 μm/layer), and 3-times higher frequency than those in the aqueduct travertine (~5 μm/layer; Supplementary Fig. 6m). Although not yet proven, the significantly thinner and higher frequency nano-layers in kidney stones (Supplementary Fig. 6) may be the result of the short-time scales over which human renal function and biochemistry can change (i.e., seconds to hours). This may also reflect the abundant and diverse sources of inhibitors in the renal environment compared to those in other geological and engineered settings. In addition, the ~140 nm-scale and finer nano-layering in CaOx kidney stones is significantly smaller than the μm-size of whole microbial cells and their associated microbial mats that directly influence layering in other geological deposits such as stromatolites[45,48]. As a result of these size constraints, kidney stone biomineralization must be controlled by some combination of human host and/or kidney microbiome derived biomolecules rather than whole cells.

CaOx kidney stones occur throughout the animal kingdom[49]. While euhedral CaOx crystals similar to COD_{FF} and COM_{FF} are also common in plants, no COM_C has yet been reported[50]. This lack of COM_C in plants likely reflects the absence of the type of high flow-through hydrodynamic environment present in the kidney, which is required to consistently deliver dissolved ions to the site of COM_C crystallization. CaOx crystallization in terrestrial plants serves to store carbon and H_2O for later use in times of reduced carbon availability and drought[50,51]. By analogy, it is also possible that COD_{FF}, COM_{FF} and even COM_C crystallization in animals may serve to store water for later use when the kidney ecosystem is stressed. *In vitro* batch reactor experiments[52], as well as our own microfluidics experimentation (Supplementary Figs. 7 and 17) to test CaOx growth dynamics, have successfully grown free-floating polymorphic COD_{FF}, COM_{FF} and their aggregates (equivalent to HSE1, Supplementary Fig. 8). While COD-to-COM and apatite-to-COM conversion has been demonstrated convincingly, no previous experimentation has grown COM_C with nano-layer couplets[3,8,53,54].

Clinical and future implications. Human beings almost constantly create urine supersaturated with respect to CaOx, yet the question remains as to why only 1 in 11 people actually grow symptomatic kidney stones[12,15]. Our study illustrates that understanding kidney stone growth requires knowledge of not only urine chemistry, but also crystalline architecture and chemistry of the stones, as well as the biomolecules derived from the host animal, kidney itself and possibly resident microbes. The HSE (Fig. 1a,b) is a new synthesis that identifies an unexpected roadmap of therapeutic targets for prevention and treatment, which include: 1) prevent COD_{FF} and COM_{FF} aggregation and their twinning; 2) promote and maintain COD_{FF} growth, continue COD_{FF} surface dissolution, then completely dissolve COD_{FF} prior to COM_C encrustation; 3) periodically induce COD_{FF} growth during COM_C formation to create layers that can be dissolved; 4) enhance any of the later-stage HSE dissolution events; and 5) disrupt crystal, urine and biomolecule components that combine to control the switching between organic matter-rich and crystal-rich COM_C nano-layers. All of these therapeutic targets would involve the introduction of macromolecules that either inhibit or promote crystal growth and dissolution, and lead to less crystal aggregation. The development of tools to read the crystalline architecture of kidney stones in a clinical setting would allow rapid evaluation and determination of which of these interventions to pursue. It has been confirmed for over a decade that precursor forms of amorphous CaOx exist as they do in calcium carbonate and calcium phosphate biomineralization[55–57]. Through a multi-step process, these amorphous CaOx phases fully transform into CaOx crystals. Although they leave behind no obvious record of their existence, clinical interventions targeting these early upstream events of biomineralization should also be considered for the treatment of kidney stones to target these transient states to destabilize the forming crystals. Taken together, these geobiology approaches will also have a transformative impact on the study of gallstones, atherosclerosis, osteoporosis and a variety of other human biomineralization conditions that involve multiple events of crystal growth and dissolution.

Methods

Detailed methods are provided online in Supplementary Materials. *Study approval.* All methods reported in this manuscript were carried out in accordance with the basic medical research study, which was reviewed and approved by the Mayo Clinic Institutional Review Board (IRB 09-002083), and the outcomes of this study will positively affect the future management of kidney stone formers. Written informed consent was obtained from all six Mayo Clinic patient participants.

Kidney stone collection and thin sectioning. Kidney stones were collected and analyzed from all six patients by a single urologist using standard percutaneous nephrolithotomy (PCNL) procedures under sterile operating room conditions at the Mayo Clinic in Rochester, Minnesota. A line of section for thin sectioning for each stone was carefully selected under a Zeiss Axio Zoom.V16 Microscope (Carl Zeiss, Oberkochen, Germany), along the orientation that would exhibit a complete cross-section of earliest-to-latest crystalline stone growth. Photographs and descriptions were sent with the six stones to Wagner Petrographic Ltd. in Linden, Utah. Here they prepared standard-sized (24 mm × 46 mm), uncovered (no cover slip), doubly polished thin sections.

Stones were first vacuum impregnated and then mounted on borate silicate glass slides with clear low-viscosity cathodoluminescence-resistant epoxy impregnation to prepare double-sided polished, 20 µm-thick petrographic thin sections.

Thin section imaging. Thin sections were imaged on a wide variety of optical modalities (Supplementary Fig. 11). A Zeiss Axio Observer system (Carl Zeiss, Oberkochen, Germany) with a Zeiss Axiocam 512 MRc was used to capture the BF, POL, PC, POLPC, CPOL, CPOLPC and WAF images across a broad range of magnifications (10x: 0.3 NA; 20x: 0.8 NA; 63x: 1.4 NA; and 100x: 1.46 NA). The objectives used were Plan-Neofluar (10x), Plan-Apochromat (20–63x) and alpha Plan-Apochromat (1.46 NA). WAF was acquired in three channels, including DAPI, FITC and Rhodamine filters. The confocal auto-fluorescence and Airyscan super-resolution nano-layers observed in the samples were investigated and quantified using a Zeiss LSM 880 Laser Scanning Microscope with Airyscan Super-Resolution. A spectral confocal system (Zeiss LSM 710) with a spectral PMT detector AF emissions and a TPAF spectral imaging, a secondary complementary FLIM technique (Fast FLIM, ISS, Champaign, IL) were used to distinguish the AF emissions produced by organic matter trapped within the calcium oxalate crystals, from those produced by the epoxy required to impregnate and mount the stones. All images were processed using the Zeiss Zen Blue and/or Black software to display either minimum and maximum or best-fit properties unless otherwise stated in the figure legends. In addition, red-green-blue (RGB) curves were adjusted individually or together to highlight all the crystal intensities in individual frames across the whole specimen. Where required, a non-linear gamma correction of 0.45 or 0.70 was applied to enhance faint AF crystal intensities in the same Zen program under the spline display mode property and all other corrections are presented in the corresponding figure legends themselves. Final images were cropped, resized and assembled using Adobe Photoshop (Adobe Systems Inc., San Jose, CA) to fit the required format. Adjustment and correction models for all images are reported in Supplementary Figs. 18–22.

Elemental analysis of kidney stones. Elemental analysis of kidney stones was performed under standard Mayo Clinic infra-red spectral analyses protocol. To qualitatively determine chemical composition, samples were analyzed with energy dispersive x-ray spectroscopy (EDXS) using an FEI Quanta FEG 450 FESEM (Hillsboro, OR).

In Vitro COM and COD crystal formation in a microfluidic device. A pilot study of initial kidney stone nidus crystal growth (HSE 1, Fig. 1) was conducted using a silica microfluidic device designed with a pore-structure design that mimics the renal calyx and pelvis environments. A solution of 0.5% (w/v) of kidney stone particles and urine was prepared and injected into the micromodel at a flowrate of 100 µl/h for 24 hrs. After this, a laboratory urine solution containing both calcium (Ca^{2+}) and oxalate ($C_2O_4^{2-}$) concentrations of 1 mM each (pH of 7.2) was prepared and injected into the micromodel at a rate of 100 µL/h to promote crystal formation in the micromodel. CaOx crystal growth was tracked with a Nikon Eclipse Ti-E epi-fluorescent inverted microscope with an Andor Zyla color camera attachment. Mineralogy of the COM and COD crystals that precipitated within in the micromodel was confirmed with Raman Spectroscopy (LabRam HR Evolution NIR, Horiba Scientific) collected between 0–1600 cm^{-1} with a 532 nm DPSS laser and confirmed with the RRUFF online database.

Data Availability

All raw data images from the microscope and point-by-point Excel spreadsheet data for FFT and line tracing graphs can be downloaded from the open access website https://figshare.com from the following links: Main Figures Raw Data Link: https://figshare.com/s/d130f7175e0266a62b97. Supplementary Raw Files Link: https://figshare.com/s/9d68faada43222c96a52.

References

1. Fourcroy, A. F. Mémoire sur le nombre, la nature et les caractères distinctifs des différents matériaux qui forment les calculs, les bézoards et les diverses concrétions des animaux. *Ann Museum* **1**, 93–113 (1802).
2. Moran, M. E. *Urolithiasis-A comprehensive history*. (Springer, 2014).
3. Beale, L. S. *Illustrations of the Constituents of Urine Urinary Deposits, and Calculi*. (John Churchill, 1858).
4. Ord, W. M. & Shattock, S. G. On the microscopic structure of urinary calculi of oxalate of lime. *Trans Path Soc London* **46**, 91–132 (1895).
5. Randall, A. Analysis of urinary calculi through the use of the polarizing microscope. *J Urol* **48**, 642–649 (1942).
6. Jensen, A. T. On concrements from the urinary tract. II. *Acta chirurgica Scandinavica* **84**, 207–225 (1940).
7. Cifuentes Delatte, L., Rapado, A. & Hodgkinson, A. Urinary Calculi. Recent Advances in Aetiology, Stone Structure and Treatment. (S. Karger, 1973).
8. Hosli, P. O. *Uber Genese und Aufbau von Harnsteinen; Inaug. Diss. Zurich*. (1957).
9. Schubert, G. & Brien, G. Crystallographic investigations of urinary calcium oxalate calculi. *Int Urol Nephrol* **13**, 249–260 (1981).
10. Prien, E. L. & Frondel, C. Studies in urolithiasis: I. The composition of urinary calculi. *J Urol* **57**, 949–994 (1947).
11. Finlayson, B. & Reid, F. The expectation of free and fixed particles in urinary stone disease. *Invest Urol* **15**, 442–448 (1978).
12. Khan, S. R. *et al*. Kidney stones. *Nature Reviews Disease Primers* **2**, 1–22, https://doi.org/10.1038/nrdp.2016.8 (2016).
13. Schwaderer, A. L. & Wolfe, A. J. The association between bacteria and urinary stones. *Ann Transl Med* **5**, 32, https://doi.org/10.21037/atm.2016.11.73 (2017).
14. Sokol, E., Nigmatulina, E., Maksimova, N. & Chiglintsev, A. $CaC_2O_4 \bullet H_2O$ spherulites in human kidney stones: morphology, chemical composition, and growth regime. *European Journal of Mineralogy* **17**, 285–295 (2005).
15. Evan, A. P., Worcester, E. M., Coe, F. L., Williams, J. Jr & Lingeman, J. E. Mechanisms of human kidney stone formation. *Urolithiasis* **43**, 19–32, https://doi.org/10.1007/s00240-014-0701-0 (2015).
16. Sivaguru, M. *et al*. Comparative performance of airyscan and structured illumination superresolution microscopy in the study of the surface texture and 3D shape of pollen. *Microsc Res Tech*. https://doi.org/10.1002/jemt.22732 (2016).
17. Sivaguru, M., Mander, L., Fried, G. & Punyasena, S. W. Capturing the surface texture and shape of pollen: a comparison of microscopy techniques. *PLoS One* **7**, e39129, https://doi.org/10.1371/journal.pone.0039129 (2012).

18. Goldraij, A. *et al*. Compartmentalization of S-RNase and HT-B degradation in self- incompatible Nicotiana. *Nature* **439**, 805–810, https://doi.org/10.1038/nature04491 (2006).
19. Laudan, R. From Mineralogy to Geology: The *Foundations of a Science*, 1650–1830. (University of Chicago Press, Chicago, 1987).
20. Craig, J. R. and Vaughan, D. J. *Ore Microscopy and Ore Petrography*. 434 p (John Wiley & Sons, 1994).
21. Williams, J. C. Jr, McAteer, J. A., Evan, A. P. & Lingeman, J. E. Micro-computed tomography for analysis of urinary calculi. *Urol Res* **38**, 477–484 (2010).
22. Daudon, M. *et al*. Composition des calculs observés aujourd'hui dans les pays non industrialisés [Composition of renal stones currently observed in non-industrialized countries]. *Progres En Urologie* **14**, 1151–1161 (2004).
23. Kim, K. M. & Johnson, F. B. Calcium oxalate crystal growth in human urinary stones. *Scan Electron Microsc* **1981-III**, 147–154 (1981).
24. Bathurst, R. G. C. *Carbonate sediments and their diagenesis*. (Elsevier, 1971).
25. Stumm, W. & Morgan, J. J. *Aquatic Chemistry*. 1040 (John Wiley & Sons, 2012).
26. Chan, B. P. *et al*. On the catalysis of calcium oxalate dihydrate formation by osteopontin peptides. *Colloids Surf B Biointerfaces* **96**, 22–28, https://doi.org/10.1016/j.colsurfb.2012.03.015 (2012).
27. Cloutier, J., Villa, L., Traxer, O. & Daudon, M. Kidney stone analysis: "Give me your stone, I will tell you who you are!". *World J Urol* **33**, 157–169 (2014).
28. Khan, S. R. & Hackett, R. L. Role of organic matrix in urinary stone formation: an ultrastructural study of crystal matrix interface of calcium oxalate monohydrate stones. *J Urol* **150**, 239–245 (1993).
29. Evan, A. P. *et al*. Randall's plaque of patients with nephrolithiasis begins in basement membranes of thin loops of Henle. *J Clin Invest* **111**, 607–616 (2003).
30. Linnes, M. P. *et al*. Phenotypic characterization of kidney stone formers by endoscopic and histological quantification of intrarenal calcification. *Kidney Int* **84**, 818–825, https://doi.org/10.1038/ki.2013.189 (2013).
31. Wang, X. *et al*. Distinguishing Characteristics of Idiopathic Calcium Oxalate Kidney Stone Formers with Low Amounts of Randall's Plaque. *Clin J Am Soc Nephrol* **9**, 1757–1763, https://doi.org/10.2215/cjn.01490214 (2014).
32. Evan, A. Physiopathology and etiology of stone formation in the kidney and the urinary tract. *Pediatric Nephrology* **25**, 831–841 (2010).
33. Lieske, J. C., Norris, R., Swift, H. & Toback, F. G. Adhesion, internalization and metabolism of calcium oxalate monohydrate crystals by renal epithelial cells. *Kidney Int.* **52**, 1291–1301 (1997).
34. Guo, S. W., Ward, M. D. & Wesson, J. A. Direct visualization of calcium oxalate monohydrate crystallization and dissolution with atomic force microscopy and the role of polymeric additives. *Langmuir* **18**, 4284–4291 (2002).
35. Wesson, J. A. & Ward, M. D. Role of crystal surface adhesion in kidney stone disease. *Curr Opin Nephrol Hypertens* **15**, 386–393 (2006).
36. Perinpam, M. *et al*. Plasma oxalate in relation to eGFR in patients with primary hyperoxaluria, enteric hyperoxaluria and urinary stone disease. *Clin Biochem*, https://doi.org/10.1016/j.clinbiochem.2017.07.017 (2017).
37. Ryall, R. L. Urinary inhibitors of calcium oxalate crystallization and their potential role in stone formation. *World J Urol* **15**, 155–164 (1997).
38. Coe, F. L., Evan, A. P. & Worcester, E. M. Kidney stone disease. *J Clin Invest* **115**, 2598–2608 (2005).
39. Khan, S. R. & Hackett, R. L. Role of scanning electron microscopy and x-ray microanalysis in the identification of urinary crystals. *Scanning Microsc* **1**, 1405–1411 (1987).
40. Evan, A. P., Coe, F. L., Lingeman, J. E. & Worcester, E. M. Insights on the pathology of kidney stone formation. *Urol Res* **33**, 383–389 (2005).
41. Evan, A. P. *et al*. Mechanism of formation of human calcium oxalate renal stones on Randall's plaque. *Anat Rec* **290**, 1315–1323 (2007).
42. Shore, M. & Fowler, A. D. Oscillatory zoning in minerals: A common phenomenon. *Can Mineral* **34**, 1111–1126 (1996).
43. Erickson, S. B., Vrtiska, T. J., Canzanello, V. J. & Lieske, J. C. Cystone(R) for 1 year did not change urine chemistry or decrease stone burden in cystine stone formers. *Urol Res* **39**, 197–203, https://doi.org/10.1007/s00240-010-0334-x (2011).
44. Evans, K. & Costabile, R. A. Time to development of symptomatic urinary calculi in a high risk environment. *J Urol* **173**, 858–861, https://doi.org/10.1097/01.ju.0000152578.07262.1c (2005).
45. Fouke, B. W., T. Murphy. *The Art of Yellowstone Science: Mammoth Hot Springs as a Window on the Universe*. 300 (Crystal Creek Press, 2016).
46. Zhou, J. Z. *et al*. Geochemistry of speleothem records from southern Illinois: Development of (U-234)/(U-238) as a proxy for paleoprecipitation. *Chem Geol* **221**, 1–20, https://doi.org/10.1016/j.chemgeo.2005.02.005 (2005).
47. Motta, D., Keenan-Jones, D., Garcia, M. H. & Fouke, B. W. Hydraulic Evaluation of the Design and Operation of Ancient Rome's Anio Novus Aqueduct. *Archaeometry* **59**, 1150–1174, https://doi.org/10.1111/arcm.12303 (2017).
48. Spear, J. R. & Corsetti, F. A. The evolution of geobiology in the context of living stromatolites. *Geol Soc Am Spec Pap* **500**, 549–565, https://doi.org/10.1130/2013.2500(17) (2013).
49. Osborne, C. A. *et al*. Quantitative Analysis of 4468 Uroliths Retrieved from Farm Animals, Exotic Species, and Wildlife Submitted to the Minnesota Urolith Center: 1981 to 2007. *The Veterinary clinics of North America. Small animal practice* **39**, 65–78 (2009).
50. Hartl, W. P. *et al*. Diversity of calcium oxalate crystals in Cactaceae. *Can J Bot* **85**, 501–517, https://doi.org/10.1139/B07-046 (2007).
51. Tooulakou, G. *et al*. Alarm Photosynthesis: Calcium Oxalate Crystals as an Internal CO_2 Source in Plants. *Plant Physiol* **171**, 2577–2585, https://doi.org/10.1104/pp.16.00111 (2016).
52. Zhao, Z., Xia, Y., Xue, J. & Wu, Q. Role of E.coli-Secretion and Melamine in Selective Formation of $CaC_2O_4.H_2O$ and $CaC_2O_4.2H_2O$ Crystals. *Crystal Growth & Design* **14**, 450–458 (2014).
53. Hesse, A., Berg, W., Schneider, H. J. & Hienzsch, E. A contribution to the formation mechanism of calcium oxalate urinary calculi. II. *In Vitro* Experiments Concerning the Theory of the Formation of Whewellite and Weddellite Urinary Calculi. *Urological Research* **4**, 157–160 (1976).
54. Khan, S. R. & Hackett, R. L. Crystal-matrix relationships in experimentally induced urinary calcium oxalate monohydrate crystals, an ultrastructural study. *Calcif Tissue Int* **41**, 157–163 (1987).
55. Gebauer, D., Volkel, A. & Colfen, H. Stable prenucleation calcium carbonate clusters. *Science* **322**, 1819–1822, https://doi.org/10.1126/science.1164271 (2008).
56. Hajir, M., Graf, R. & Tremel, W. Stable amorphous calcium oxalate: synthesis and potential intermediate in biomineralization. *Chem Commun (Camb)* **50**, 6534–6536, https://doi.org/10.1039/c4cc02146k (2014).
57. Ruiz-Agudo, E. *et al*. A non-classical view on calcium oxalate precipitation and the role of citrate. *Nat Commun* **8**, 768, https://doi.org/10.1038/s41467-017-00756-5 (2017).

Acknowledgements

Kidney stone samples were collected following Mayo Clinic Institutional Review Board approval (IRB 09-002083) and written patient consent. This research was supported by the Mayo Clinic and University of Illinois Strategic Alliance for Technology-Based Healthcare, the Mayo Clinic O'Brien Urology Research Center (No. DK100227), the Mayo Special Undergraduate Research Fellowship (SURF), and the National Aeronautics and Space

Administration (NASA) Astrobiology Institute (Cooperative Agreement No. NNA13AA91A) issued through the Science Mission Directorate. K. Lee conducted EDXS analyses at the Illinois Beckman Institute. We thank G. Robinson, N. Goldenfeld, B. White, Y. Dong, A. Merkel, J. Webber, M. Cregger, M. Baughman, L. Shechtman, E. Wilson, M. Casagrande, B. Sivaguru, V. Sivaguru, L. Nazal, T. Rauschfuss, D. Bish and B. Michelson for their contributions in editing the final manuscript and/or sample preparation.

Author Contributions

M.S., J.J.S., B.W.F. performed the experiments and analyzed the data, M.S., and J.S. prepared final images. J.C.W. collected and provided MicroCT data. A.E.K. performed the PCNL-isolation of all kidney stones reported in this manuscript from Mayo Clinic patients. R.E.A. and C.J.W. performed *in vitro* experiments of kidney stones and provided results of early stages of crystal formation. M.S. drafted and wrote the manuscript. B.W.F. edited the initial draft and supervised the project. M.S., J.J.S., J.C.W., J.C.L., A.E.K., M.F.R., N.C., A.L.S., R.E.A., W.J.B., D.E.W., G.A.F., C.J.W., R.J.R., P.Y., R.A.S. and B.W.F. provided collaborative research support throughout the study, reviewed and edited the central parts of the initial manuscript made available by M.S., J.J.S., J.C.W. and B.W.F. in their respective fields of expertise continuously leading up to the submission version.

Additional Information

Supplementary information accompanies this paper at https://doi.org/10.1038/s41598-018-31890-9.

Competing Interests: The authors declare no competing interests.

Publisher's note: Springer Nature remains neutral with regard to jurisdictional claims in published maps and institutional affiliations.